Identification of Eschweilenol C in derivative of *Terminalia fagifolia* Mart. and green synthesis of bioactive and biocompatible silver nanoparticles

Alyne Rodrigues de Araujo[a,b], Joilson Ramos-Jesus[b], Taiane Maria de Oliveira[b], Andressa Maria A. de Carvalho[c], Paulo Humberto M. Nunes[d], Tatiane Caroline Daboit[c], Ana P. Carvalho[e], Maria Fátima Barroso[e], Miguel Peixoto de Almeida[f], Alexandra Plácido[g,h], Artur Rodrigues[g], Camila C. Portugal[g], Renato Socodato[g], João B. Relvas[g], Cristina Delerue-Matos[e], Durcilene Alves da Silva[a,b], Peter Eaton[f], José Roberto de Souza de A. Leite[b,i,*]

[a] *Programa de Pós-Graduação em Biotecnologia, RENORBIO, Brazil*
[b] *Núcleo de Pesquisa em Biodiversidade e Biotecnologia, BIOTEC, UFPI, Parnaíba, PI, Brazil*
[c] *Grupo de Estudos Avançados em Micologia Médica, GEAMICOL, UFPI, Parnaíba, PI, Brazil*
[d] *Núcleo de Pesquisa em Plantas Medicinais, NPPM, UFPI, Teresina, PI, Brazil*
[e] *LAQV/REQUIMTE, Instituto Superior de Engenharia, Instituto Politécnico do Porto, Portugal*
[f] *LAQV/REQUIMTE, Departamento de Química e Bioquímica, Faculdade de Ciências, Universidade do Porto, Portugal*
[g] *Instituto de Investigação e Inovação em Saúde (i3S) e Instituto de Biologia Molecular e Celular, IBMC, Porto, Portugal*
[h] *Bioprospectum, Lda, UPETC, Porto, Portugal*
[i] *Nucleo de Pesquisa em Morfologia e Imunologia Aplicada, NuPMIA, Area Morfologia, Faculdade de Medicina, Universidade de Brasília (UnB), Brasília, Brazil*

A B S T R A C T

A green synthetic route was developed to prepare silver nanoparticles (AgNPs) in aqueous solution for biological applications. Eschweilenol C, a compound derivative ellagic acid was identified as the main constituent of the aqueous fraction of the ethanolic extract of *Terminalia fagifolia* Mart. by NMR analysis. In the green synthesis, the ethanolic extract of *T. fagifolia* and its aqueous fraction were used to promote silver reduction and nanoparticle stabilization. The synthesized AgNPs presented a spherical or polygonal morphology shape by TEM analysis and AgNPs showed high levels of antioxidant and considerable antibacterial and antifungal activities. Synthesized nanoparticles presented significant antioxidant activity by sequestration of DPPH and ABTS radicals, in addition to iron reduction (FRAP assay) and measurement of antioxidant capacity in ORAC units, in addition, AgNP synthesized with the aqueous fraction also demonstrated antioxidant potential in microglial cells. Gram-positive and Gram-negative bacteria were susceptible to growth inhibition by the nanoparticles, among which the AgNPs formed by the ethanolic extract was the most effective. The data obtained by AFM images suggested that AgNPs could lead to the lysis of bacteria and subsequent death. The antifungal assays showed high efficiency against yeasts and dermatophytes. This work represents the first description of antifungal activity by AgNPs against *Fonsecaea pedrosoi*, the etiologic agent of chromoblastomycosis. In relation to biocompatibility, the AgNPs induced lower haemolysis than $AgNO_3$.

Keywords:
Ellagic acid
Metallic nanoparticles
Terminalia sp.
Antioxidant
Antimicrobial
Fonsecaea pedrosoi

1. Introduction

Despite efforts to discover new drugs for the treatment of infectious diseases, pathogens have shown versatility in the development of several antimicrobial resistance mechanisms. Infectious diseases remain a recognized worldwide health problem and, in this context,

Abbreviations: EtE, the ethanolic extract of stem bark from *Terminalia fagifolia* Mart; AgNPEtE, silver nanoparticles formed with the ethanolic extract of stem bark from *Terminalia fagifolia* Mart; AqF, the aqueous fraction of the ethanolic extract of stem bark from *Terminalia fagifolia* Mart; AgNPAqF, silver nanoparticles formed with the aqueous fraction of the ethanolic extract of stem bark from *Terminalia fagifolia* Mart; ROS, reactive oxygen species

* Corresponding author at: Universidade de Brasília, UNB, Area of Morphology, Faculty of Medicine, FM, CampusDarcy Ribeiro, Asa Norte, University of Brasilia (UnB), 70910900, Brazil.
E-mail addresses: jrsaleite@gmail.com, jrleite@pq.cnpq.br (J.R. de Souza de A. Leite).

antimicrobial resistance is an important phenomenon which complicates the treatment and cure these illnesses. In addition, some medical treatment options for complicated infections include combinations of drugs, which are associated with significant adverse effects and do not guarantee entirely satisfactory results (Lin et al., 2015; WHO, 2018).

In previous research, we have demonstrated antimicrobial potential of the extracts and fractions from *Terminalia fagifolia* Mart. as well as other biological activities. In many cases, biological activities and properties of natural compounds may be improved by incorporation in a nanostructured system. In this context, the antimicrobial activity of silver nanoparticles is noteworthy, since microbes generally have greater difficulty in developing resistance to silver when compared to antibiotics (Nunes et al., 2014; Araújo et al., 2015; Durán et al., 2016).

Metal nanoparticles are among the most widely-applied nanomaterials, in particular, silver nanoparticles (AgNPs) possess a number of useful properties including moderate chemical stability and strong biological interactions, including antibacterial, antifungal and antioxidant activities, with decrease of reactive oxygen species (ROS) in microglia (resident immune cells of the brain). Because of this, AgNPs are among the most widely used nanomaterials in consumer products (Tolaymat et al., 2010; Gonzalez-Carter et al., 2017).

Green synthesis of nanoparticles, also known as biological synthesis, is a simple, low-cost, eco-friendly and scalable procedure, facilitating economic viability and sustainable synthesis. In this context, green synthesis of nanoparticles using plant derivatives is an emerging area of nanotechnology that usually involves a single step of reduction (Kuppusamy et al., 2016). The use of plant extracts holds some advantages such as good accessibility to plant material and low biological risk. Moreover, the use of regionally endemic plants can strengthen the local production chain, and reduce emissions (Kalishwaralal et al., 2010). Relatively high levels of secondary metabolites, such as phenolic compounds, can act as reducing agents and as nanoparticle capping agents, providing stability and biological compatibility (Sun et al., 2014).

Plants of the genus *Terminalia* range from shrubs to large trees and are rich in several secondary metabolites, which explains their wide use in folk medicine. *Terminalia fagifolia* is a melliferous tree found in the Brazilian cerrado, used by the local population for the treatment of canker sores and tumours (Nunes et al., 2009; Cock, 2015).

Research published by Nunes et al (2014) suggests the presence of catechin and epicatechin in the ethanolic extract of *T. fagifolia* Mart., but did not elucidate the major compound of the aqueous fraction from ethanolic extract, that showed better biological activities in some published data. This study reports for the first time, the major constituent of the aqueous fraction of the ethanolic extract of *T. fagifolia* and describes the green synthesis of silver nanoparticles with derivatives of *T. fagifolia*, as well as the evaluation of their biological activities.

2. Material and methods

2.1. Collection of plant materials, preparation and partition of the ethanolic extract

The stem bark of *T. fagifolia* was collected in Timon city, Maranhão State, Brazil. A voucher specimen was deposited in the Graziela Barroso Herbarium, UFPI, with number 21,691. The plant material was shade-dried, and the stem bark powder was extracted with 99.6% ethanol or 50% hydroalcoholic solution at room temperature. After filtration, the solvents were eliminated and the concentrates were lyophilized to obtain the dry *T. fagifolia* ethanolic extract (EtE). To obtain the partition fraction of EtE, it was dissolved in a methanol/distilled water solution (1:2 *v/v*) and extracted with ethyl acetate. After this time, the ethyl acetate phase was concentrated and dissolved in a methanol/distilled water solution (9:1 *v/v*). The phases obtained were concentrated and one of them resulted in the aqueous fraction (AqF) of EtE (Nunes et al., 2014).

2.2. Preparation of samples for NMR and LC–MS analysis

For identification of the major constituent of the aqueous fraction of the ethanolic extract of *T. fagifolia*, the isolated molecule was obtained by high performance liquid chromatography on hybrid equipment composed of a binary pump system (HPLC, Shimadzu, Tokyo - Japan) equipped with Phenomenex-Luna C_{18} column (4 µm) and UV–vis detector, using a gradient of 0.1% formic acid and acetonitrile with 0.1% trifluoroacetic acid (Sigma-Aldrich).

2.3. NMR and LC–MS analysis

NMR spectra were recorded on a BRUKER AVIII-600 MHz NMR spectrometer equipped with a cryogenically cooled triple resonance probe. The sample isolated by HPLC was dissolved in 525 µL DMSO-d6 (99.8% D, containing 0.03% *v/v* TMS, Sigma-Aldrich). All NMR spectra were recorded at 308.1 K. Spectra were referenced to internal TMS. TopSpin 3.5pl6 was used for recording and processing data. For the LC–MS analysis, 5 µL of the NMR sample was analysed on a BRUKER compact ESI-qTOF mass spectrometer connected to a Hitachi LaChrome Elite HPLC equipped with a C_{18} column (Ascentis Xpress, 2.7 µm) kept at 40 °C. Elution was performed with a gradient starting at 10% Acetonitrile and 90% water (both LC–MS grade, supplemented with 0.1% formic acid), and linearly increasing to 100% Acetonitrile with 0.1% formic acid. In addition to the mass spectrometer, the HPLC system was also equipped with a Hitachi LaChrome Elite L-2450 DAD UV-detector.

2.4. Synthesis of silver nanoparticles (AgNPs)

Silver nanoparticles were synthesized by a one-step reduction. Briefly, the $AgNO_3$ precursor (1 mM) (Sigma-Aldrich) was dissolved in water and freshly prepared solutions of *T. fagifolia* stem bark extract and fraction (0.2% *w/v*) freshly prepared was mixed (1:1 *v/v*) to obtain a final concentration of 500 µMAg and 0.1% of extract and fraction, then the solutions obtained were stirred for 72 h at room temperature.

2.5. Particle characterizations

AgNPs were characterized using ultraviolet–visible spectroscopy (UV-1800, Shimadzu, Japan) in the range 300–600 nm. The functional groups were studied using Fourier transform infrared spectroscopy (FTIR- Shimadzu IRAffinity-1S, Japan) in the spectral range from 4000 to 700 cm^{-1} resolution. Transmission electron microscopy - TEM/EDS (using either a Hitachi H7000 TEM at 100 kV or a JEOL JEM 1400 also at 100 kV) was performed to study the surface morphology and size of the AgNPs, and confirm the composition. Zeta potential and mean size were measured using Malvern Zeta Sizer analyzer by dynamic light scattering method (DLS). Nanoparticle tracking analysis – NTA (Malvern NanoSight NS300, using NTA 3.2 software) was performed to observe the particle concentration and mean size of the AgNPs using a 542 nm laser.

2.6. Antioxidant activity tests

The antioxidant capacity of the AgNPs was studied *via* measurement of free radical scavenging, using the cation radicals $ABTS^{\cdot+}$ (2,2′-azinobis (3-ethylbenzthiazoline-6-sulfonic acid) and DPPH, according to Gião et al. (2007) and Barroso et al. (2016), respectively. The ferric reduction antioxidant power (FRAP) assay (Barroso et al., 2016) and oxygen radical absorbance capacity (ORAC) assays were also performed (Huang et al., 2002). The total phenolic content (TPC) of AgNPs, extracts and fractions was determined using the Folin–Ciocalteau reagent. A Multi-Mode Microplate Reader (BioTek Instruments, Inc., USA) was

used to perform these measurements.

2.7. LPS-induced ROS production in living microglia cells

The human microglial cell line CHME3 was obtained from primary cultures of human embryonic microglial cells by transfection with a plasmid encoding for the large T antigen of SV40 and were cultivated as before mentioned by Barbosa et al. (2018). For the assays, microglia were transiently transfected with HyperRed ROS biosensor, using Jetprime (Polyplus), according to manufacturer's. Experiments were performed on a DMI6000B microscope (Leica Microsystems) equipped with a near infra-red filter cube. Microglial cells were recorded for 10 min in normal saline or saline with AqF at concentration of 125 μg/mL or AgNPAqF (27 μgAg/mL) for baseline. Then the groups were recorded in the presence of lipopolysaccharide - LPS (1 μg/mL) for 30 min (stimulation period). Time-lapse images were exported and processed in the FIJI software, and values corresponding to whole biosensor mean gray intensity were retrieved as before (Barbosa et al., 2018).

2.8. Electrochemical analysis

Differential pulse voltammetry experiments were performed with an Autolab PGSTAT128 N Potentiostat/Galvanostat (EcoChemie, Utrecht, The Netherlands) using NOVA 1.6 Software. A three electrode configuration was used, comprising of a screen-printed carbon electrode (SPCE), which integrates the working carbon electrode, an auxiliary carbon electrode and a reference silver electrode. Buffer solutions containing gallic acid (1 mg/mL) and quercetin (1 mg/mL) were used as model analytes. The standard buffer solution was a 0.1 M HCl, at pH 4.3. For the voltammetric determination, an aliquot of 5 μL of sample plus 45 μL of buffer was added to the working electrode surface. Then, a constant potential of −0.2 V was applied for 180 s in order to preconcentrate the ions at the working electrode surface. After that, the potential was swept from −0.2 V to +1.0 V using differential pulse voltammetry to strip the ions back into the solution. All the eletrochemical experiments were carried out in triplicate and at room temperature.

2.9. Antibacterial activity tests

The antibacterial activity was studied by determining the lowest concentration of nanoparticles capable of inhibiting bacterial growth (MIC) according to Clinical Laboratory Standards Institute, CLSI (2012), with modifications (Quelemes et al., 2013). AgNPs were tested against Gram-positive bacteria strains *Staphylococcus aureus* (ATCC® 29213™), *Staphylococcus aureus* (ATCC® 43300™ Methicillin Resistant, MRSA), *Enterococcus faecalis* (ATCC® 29212™); and the Gram-negative strains *Escherichia coli* (ATCC® 25922™), *Pseudomonas aeruginosa* (ATCC® 27853™) and *Salmonella enterica* subsp. *enterica* serovar Typhimurium (ATCC® 14028™). The bacteria were exposed to two-fold serial dilution of the AgNPs and $AgNO_3$ (positive control) ranging from 0.84 to 27 μgAg/mL in Mueller-Hinton broth (Difco™). Standard antibiotics effective against the bacterial also were used as positive control (32 to 0.25 μg/mL).

2.10. Study of the effect of AgNPEtE on the structure of bacteria by atomic force microscopy (AFM)

Morphological analysis of the *E. coli* ATCC 25922 after treatment with AgNPEtE was carried out using a TT-AFM instrument (AFM Workshop, USA) in vibrating (tapping) mode with 512 × 512 lines (6 μm × 6 μm). Prior to AFM analysis, a MIC assay was performed as previously described. After the incubation period (24 h), 20 μL of the culture media containing the sub-MIC (0.5 MIC) and AgNP-treated or untreated bacteria were applied on a clean surface, then the samples were dried at room temperature for 20 min. To complete the preparation of the samples, deionized water was used to remove the salts. Images were made using ACT-20 cantilevers (AppNano, USA) with tip radius < 10 nm and a resonant frequency of approximately 359 kHz, representative images were analysed using Gwyddion 2.47 software tools.

2.11. Antifungal activity tests

Antifungal susceptibility testing was conducted in accordance with protocols M38-A2 and M27-A3 of the Clinical and Laboratory Standards Institute, CLSI (CLSI, 2008a,b). AgNPs were tested against one yeast: *Candida krusei* ATCC® 6258™ ($5.0 \times 10^2 - 2.5 \times 10^3$ CFU/mL); and two strains of filamentous fungi: *Tricophyton interdigitale* 73826 (1×10^3 - 3×10^3 CFU/mL) and *Fonsecaea pedrosoi* ATCC® 46428™ (0.4×10^4 – 5×10^4 CFU/mL). The microorganisms were exposed to serial dilution of AgNPs or $AgNO_3$ with concentrations ranging from 0.05 to 27 μgAg/mL. The positive control standard drug, itraconazole was used in the concentration range of 0.0313–16 μg/mL. The assay was performed using 96-well plates with a U-shaped base and determination of MIC was carried out visually by comparison with the drug-free control growth.

2.12. Haemolytic activity assay

For the biocompatibility study, the haemolytic activity assay was performed using human erythrocytes, collected in tubes containing EDTA (1.8 mg/mL) by spectrophotometric measurement of haemoglobin release after exposure to various concentrations of AgNPs *in vitro*, according to Marani et al. (2016). The red blood cell (RBC) suspension (2%) was mixed with the AgNP solution and $AgNO_3$ in the concentrations of 0.84–27 μgAg/mL, the mixtures were incubated for 30 min at 35 ± 2 °C and then centrifuged at 10,000*g* for 1 min. The supernatant was separated and the absorbance value (A) measured at 492 nm in a plate reader. Triton-X (0.1% *v/v*) was used as positive control and saline solution (0.85% *w/v*) as negative haemolysis control. The haemolysis percentage (%) was calculated from equation: $[(A_{AgNP} - A_{saline})/A_{triton}\text{-}A_{saline})] \times 100$.

The data obtained were statistically analysed by two-way *ANOVA* with Tukeys's post-test using GraphPad Prism® version 6.0 (GraphPad Software Inc., San Diego, CA/USA). Significance was accepted at $p < 0.05$.

3. Results and discussion

We prepared ethanolic extract (EtE), with 19% yield, from stem bark of *T. fagifolia* (see Methods section) and the ethanolic extract was further fractionated into the aqueous fraction (AqF), with 34% yield. These materials were lyophilized and used for the studies developed.

3.1. HPLC/NMR/LC–MS analyzes

In Fig. 1, the HPLC chromatogram for AqF is presented, where we can observe two high intensity peaks. The peak with retention time of 28.183 min was collected for NMR and LC/MS analysis. Literature search for the molecular formula and the rhamnose unit already identified by NMR, led to Eschweilenol C (Fig. 2), a derivative of ellagic acid (NMR spectroscopic data are shown in Table 1. Comparison of NMR chemical shifts and the HMBC correlations (Table 2) confirmed the identity. The literature data for Eschweilenol C interchanged the chemical shifts for positions 1 and 6 (and 1´and 6´) which we could identify by the size of the J_{CH} coupling constant as detected in the HMBC spectrum. Our assignment is in agreement with data published on ellagic acid, where the chemical shift for C-6 is also downfield from C-1. The average chemical shift difference from the published values was 0.24 ppm, the maximal deviation 1 ppm (Li et al., 1999; Yang et al., 1998; Asami et al., 2003). ESI (+) TOF mass spectra gave two ions for

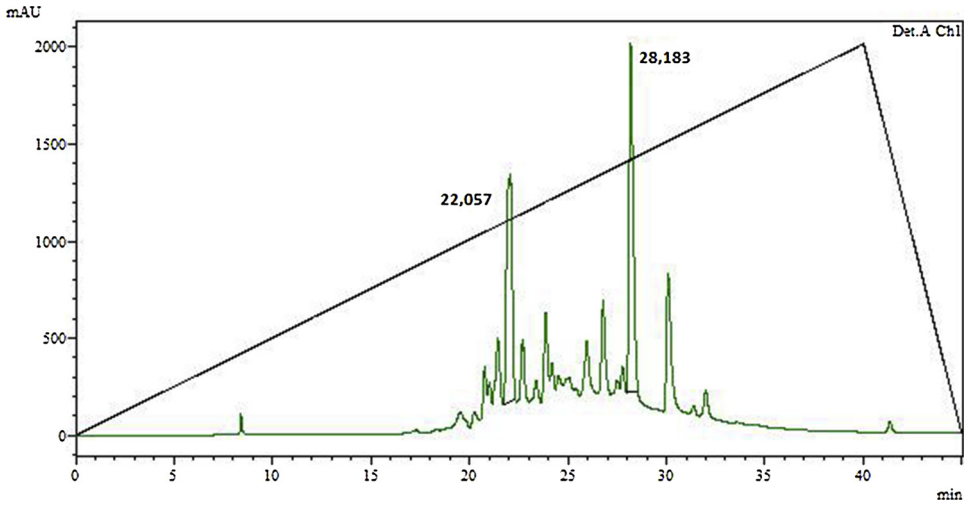

Fig. 1. HPLC chromatogram of aqueous fraction of ethanolic extract from *Terminalia fagifolia* Mart.

the compound: 303.013 and 449.071 (both for $[M+H]^+$). The difference of 146.058 Da corresponds to $C_6H_{10}O_4$, a fragment typical for a desoxy-hexose. The molecular formula then should be $C_{20}H_{16}O_{12}$ (448.064 for the neutral molecule or 449.072 for $[M+H]^+$).

3.2. Silver nanoparticle synthesis and characterization

The AgNP synthesis process was observed *via* the colour change in the reaction mixture (composed of the plant extracts and $AgNO_3$). In this study, no further purification of the nanoparticles was performed considering that purification of the nanoparticles produced by natural extracts can require processes that increases the cost, reduces yield and generates waste, besides causing instabilities of the nanoparticles (Stavis et al., 2018). A major advantage of a green synthesis method such as that described here, is the lack of toxic by products or reagents in the synthesis medium, reducing the need for further purification. The formation of nanoparticles was confirmed by UV–vis spectroscopy through the analysis of the appearance of surface plasmon resonance absorption peaks ranging between 350 and 500 nm (Salem et al., 2016). Fig. 3 shows a schematic illustration of the AgNP synthesis, as well as the visual appearance of the reported products (Fig. 3A). The UV–vis spectrum (Fig. 3B) shows, for all AgNPs colloidal solutions, a band around a wavelength of 365 nm. Although not the most common, this result is similar results were found by Rasheed et al. (2018) and Mulvaney (1996), who prepared AgNPs using Cefixime and citrate, respectively.

The broad bands formed in this region may indicate the presence of polydisperse nanoparticles, corroborating the polydispersity index (PDI) of the AgNPs, which ranged from 0.41 ± 0.01 to 0.51 ± 0.04, as can be seen in Table 3 (Rajeshkumar et al., 2013). The mean particle hydrodynamic size measured by DLS was equal to 66.2 ± 3.6 nm and 81.4 ± 1.6 nm, for AgNPEtE (silver nanoparticle synthesized with the ethanolic extract of *T. fagifolia*) and AgNPAqF (silver nanoparticle synthesized with the aqueous fraction of ethanolic extract of *T. fagifolia*), respectively. The zeta potential values (Table 3) were negative for all nanoparticles (AgNPs) and close to −30.0 mV. This large zeta potential can indicate high colloidal stability of the system due to presence of strong repulsive forces between the negatively charged particles (Rajesh et al., 2018; Salopek et al., 1992).

Although the size values for DLS and NTA were not identical, both

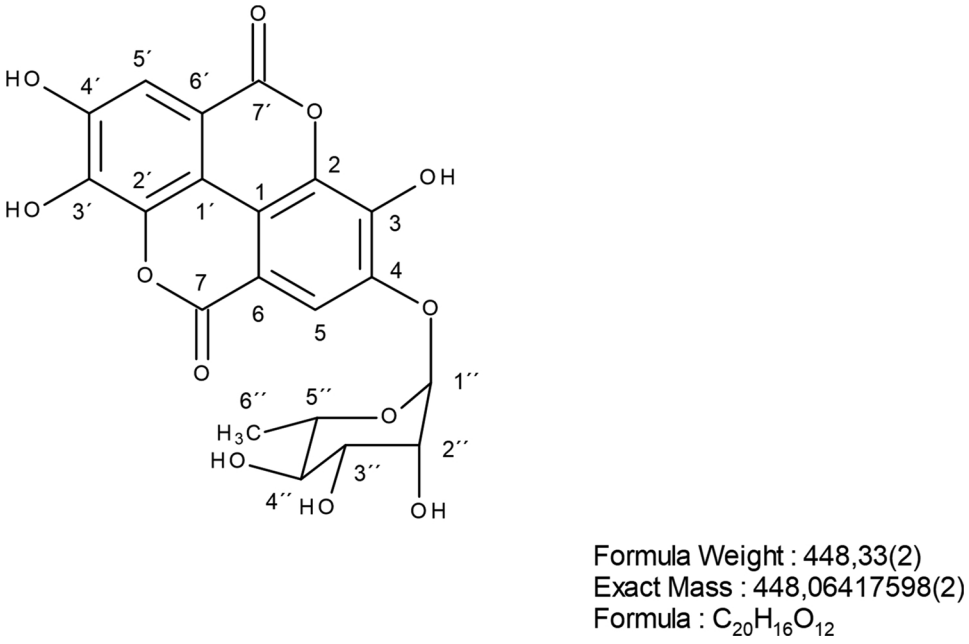

Fig. 2. The chemical structure of Eschweilenol C with numbering used in Table 1.

Table 1
NMR spectroscopic data.

Position	δ ^{1}H	Mult	δ ^{13}C	^{13}C fragment	HMBC. Correlations and assignment	δ ^{13}C Lit[#]
1			114.45	C		108.4[*]
2			136.30	C		136.8
3			141.15	C		141.0
4			146.30	C		146.4
5	7.75	s	111.55	CH	**141.15** (3), 146.31(4), **114.45** (1), 111.71(1´), 107.41(6), 136.30(2), 158.99(7)	111.7
6			107.41	C		114.6[*]
7			158.99	C		159.3
1´			111.71	C		107.8[*]
2´			136.66	C		136.5
3´			139.72	C		139.5
4´			148.68	C		148.6
5´	7.49	s	110.19	CH	136.66(2´), **139.72**(3´), 114.45(1), **111.71**(1´), 148.68(4´), 107.94(6´), 158.84(7)	110.5[*]
6´			107.94	C		112.0
7´			158.84	C		159.1
1´´	5.46	"s"	100.12	CH	146.31(4), 69.80(5´´), 69.76(2´´)	100.3
2´´	4.00	"d"	69.76	CH	71.67(4´´),	69.9
3´´	3.85	dd	70.03	CH	71.67(4´´), 69.76(2´´)	70.1
4´´	3.33	dd	71.67	CH	69.80(5´´), 69.76(2´´), 17.72(6´´)	71.8
5´´	3.57	ddq	69.80	CH	70.03(3´´), 17.72(6´´)	70.1
6´´	1.14	d	17.72	CH_3	71.67(4´´), 69.80(5´´)	18.0

[*] Positional assignment for 1 and 6 might be interchanged (Li et al., 1999).
[#] (Yang et al., 1998).

Table 2
Comparison of ^{13}C NMR chemical shifts.

Position	δ ^{13}C in DMSO[1]	δ ^{13}C in DMSO[2]	^{13}C in MeOD[2]	δ ^{13}C in DMSO own work
1	108.4[*]	106.8[*]	108.8[*]	114.45
2	136.8	136.7	137.7	136.30
3	141.0	142.0	143.0	141.15
4	146.4	146.1	147.7	146.30
5	111.7	111.6	113.5	111.55
6	114.6[*]	114.8[*]	116.1[*]	107.41
7	159.3	159.2	161.0	158.99
1´	107.8[*]	107.4[*]	109.7[*]	111.71
2´	136.5	136.6	137.8	136.66
3´	139.5	140.5	141.0	139.72
4´	148.6	148.9	150.0	148.68
5´	110.5[*]	110.0[*]	111.8[*]	110.19
6´	112.0	111.9	113.1	107.94
7´	159.1	159.1	161.0	158.84
1´´	100.3	99.6[**]	101.5[**]	100.12
2´´	69.9	69.8[**]	71.8[**]	69.76
3´´	70.1	67.6[**]	70.0[**]	70.03
4´´	71.8	73.6[**]	75.2[**]	71.67
5´´	70.1	67.4[**]	69.1[**]	69.80
6´´	18.0	17.5[**]	17.9[**]	17.72
3´´-Ac-CO		170.0[**]	172.5[**]	
3´´-Ac-CH_3		21.0[**]	21.0[**]	

[*] Positional assignment for 1 and 6 might be interchanged (Li et al., 1999).
[**] Chemical shifts are for 3´´-Acetyl Rhamnose/[1](Yang et al., 1998)/[2](Asami et al., 2003).

DLS and NTA showed similar trends: AgNPEtE (nanoparticles synthesized with extract) were the smallest nanoparticles. Although DLS and NTA both measure size *via* hydrodynamic diameter in solution, they use different measurement mechanisms and other studies have reported different results between the two techniques (Maccuspie et al., 2011). NTA measures a much smaller number of particles compared to DLS, so it's possible a fraction of much smaller particles was missed by NTA, that DLS measured. The nanoparticle concentration in solution measured by NTA was in the order of 10^{10} particles/mL and the AgNPAqF sample was approximately double the concentration of the other sample (AgNPEtE). The data from light scattering methods are shown in Table 3.

Fig. 4 shows the size distribution obtained from NTA, evidencing a relatively monodisperse population, with predominance of nanoparticles that has size around 100 nm, for the AgNPAqF (Fig. 4B), compared to the nanoparticles synthesized with the ethanolic extract – AgNPEtE, where a high degree of polydispersity was observed (Fig. 4A). This result corroborates with the PDI in the DLS analysis (Table 3), in which AgNPEtE was more polydisperse. Nevertheless, despite a majority peak of the order of 100 nm, all NTA results show the presence of a minor proportion of larger particles with diameters of the order of several hundred nanometers in solution. These could be individual larger particles, or small aggregates of particles

FTIR analysis was performed for extract, fraction and AgNPs to identify the possible involvement of the molecules present in these extracts and fractions in the process of reduction of the Ag^{+} ions. The spectra show the bands characteristic of OH stretching (3200 to 3600 cm^{-1} region) in addition to the bands of phenolic compounds present in derivatives of *T. fagifolia*: bands at 1600 cm^{-1} assigned to C=C stretching, at 1440-1450 cm^{-1} due to CH stretching, at $1100-1040\ cm^{-1}$ assigned to the vibrations of C–O of alcohols. Bands between $630-610\ cm^{-1}$ are characteristic of the C–H groups of aromatic rings. Some of these functional groups may also be present in carbohydrate residues of molecules such as Eschweilenol C (Fig. 2). While in the spectra of the AgNPs we can observe the decrease of the bands characteristic of phenolic compounds cited above, such as the band in the region of 1200 cm^{-1} (C–O of carboxylic acids, esters and ethers), the appearance of an intense band in the region of 1640 cm^{-1} that corresponds to the N–H bending of primary amines, can also be seen in Fig. 5 (Paczkowska et al., 2015; Sun et al., 2014).

Terminalia fagifolia is a plant rich in phenolic compounds, such as epicatechin and Eschweilenol C that contain high density of hydroxyl groups. These compounds can be oxidized and converted to its quinone form, then metal ions Ag^{+} are reduced to Ag^{0} followed by cluster formation until the formation of AgNPs. These quinone structures can act as agents for capping of AgNPs and play an important role in the stability of the nanoparticles. Carbohydrates such as rhamnose present in the molecule of Eschweilenol C may also contribute to the reduction and stabilization of silver ions for the formation of nanoparticles (Fig. 6) (Nunes et al., 2014; Edison et al., 2016; Suman et al., 2013).

Fig. 7 shows a heterogeneous population of nanoparticles analysed by TEM, with spherical shape (Fig. 7A/B) and hexagonal symmetry (Fig. 7C/D). The different shapes of *T. fagifolia*-AgNPs may explain the broad bands observed in UV–vis analysis, as well the PDI values above 0.4. From the EDS analysis of AgNPAqF (Fig. 8), a strong signal of the

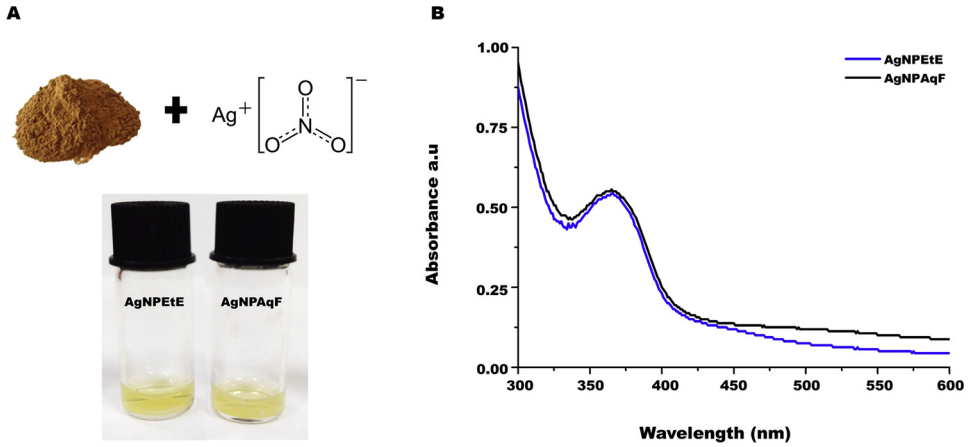

Fig. 3. Schematic illustration of the AgNP green synthesis and respective AgNPs colloidal solutions (**A**); UV–vis spectra of AgNPs solutions (**B**). (Nanoparticle synthesized with: ethanolic extract - AgNPEtE and aqueous fraction -AgNPAqF).

Table 3
Mean particle size, polydispersity index (PDI), Zeta potential and concentration of AgNPs.

AgNPs*	Mean Size (nm) by DLS	Mean Size (nm) by NTA	PDI	Zeta Potential (mV)	Concentration (particles/mL)
AgNPEtE	66.2 ± 3.6	110.2 ± 1.8	0.51 ± 0.04	−27.0−27.0 ± 5.3	$1.0 \pm 0.3 \times 10^{10}$
AgNPAqF	81.4 ± 1.6	133.8 ± 1.8	0.41 ± 0.01	−23.5 ± 5.4	$1.9 \pm 0.7 \times 10^{10}$

AgNPAqF — nanoparticles synthesized with the aqueous fraction.
* AgNPEtE — nanoparticles synthesized with the ethanolic extract.

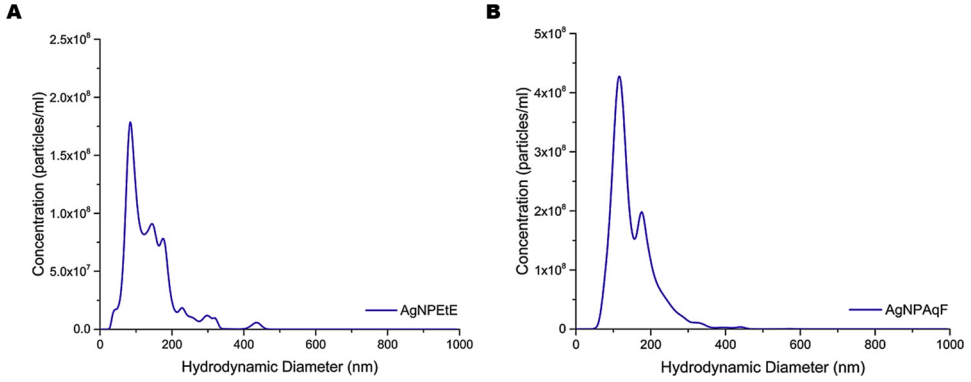

Fig. 4. Representative size distribution profiles of AgNPs from NTA measurements.

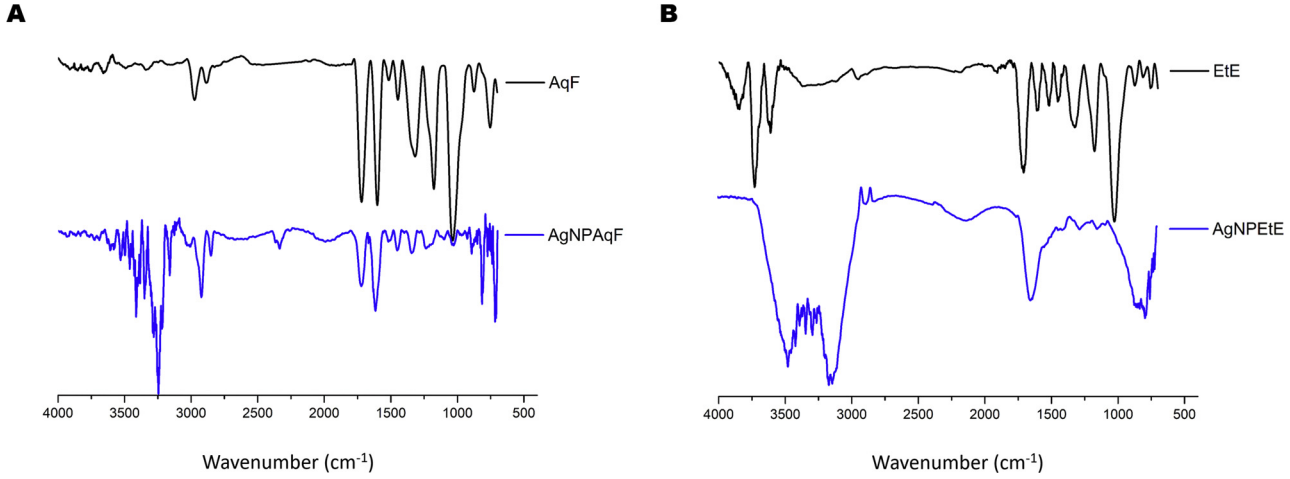

Fig. 5. FTIR spectra of the AgNPs/extracts or fractions. **A**)AgNPEtE/EtE and **B**)AgNPAqF/AqF.

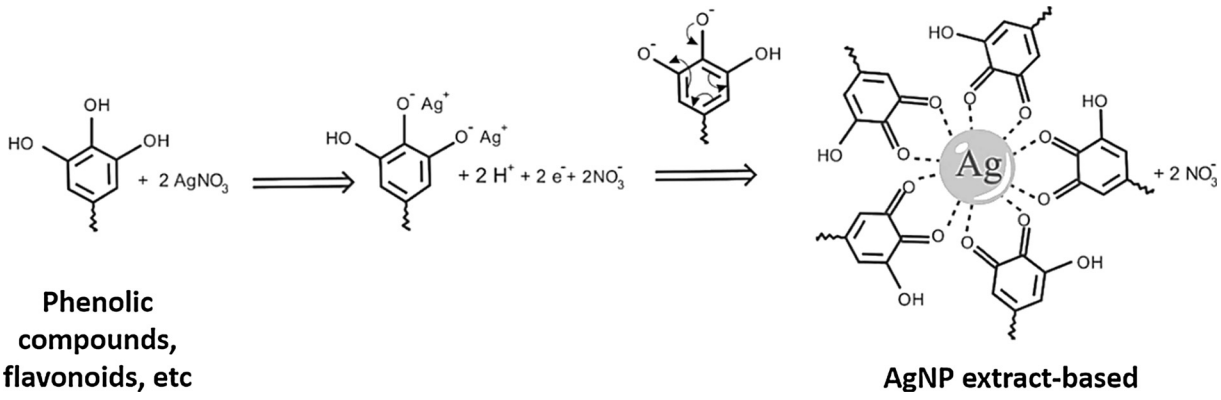

Fig. 6. Suggested mechanism of synthesis and stabilization of AgNPs based on *T. fagifolia* extracts.

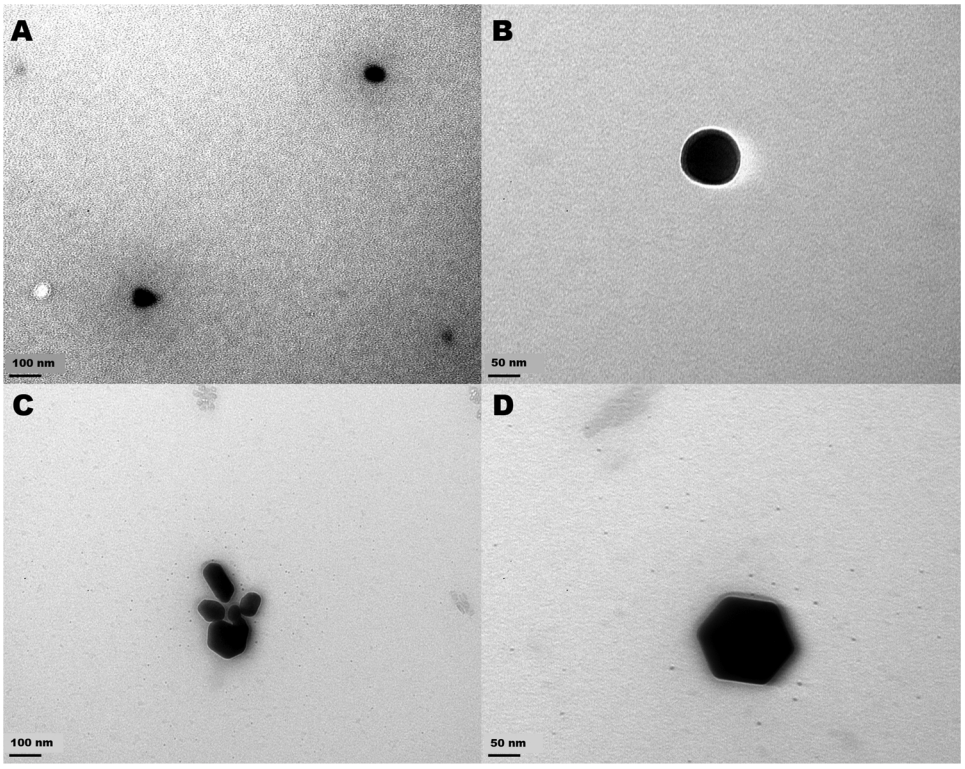

Fig. 7. TEM images illustrating the morphology of AgNPs – **A-B**) AgNPEtE and **C-D**)AgNPAqF.

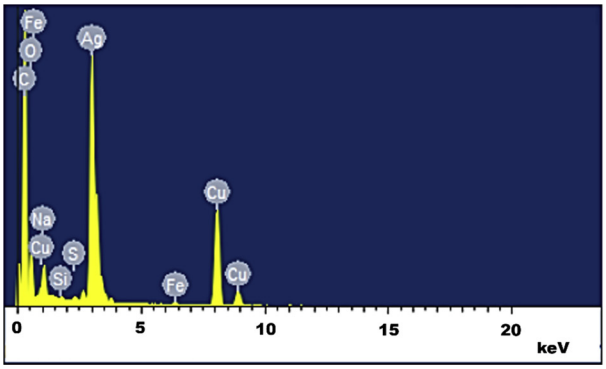

Element	Weight%	Atomic%
C K	27.28	68.90
O K	3.45	6.54
Na K	1.72	2.28
Si K	0.13	0.14
S K	0.14	0.13
Fe K	0.12	0.06
Cu K	15.58	7.44
Ag L	51.7	14.50
Totals	100.0	

Fig. 8. EDS analysis of silver nanoparticle synthesized with the aqueous fraction of *T. fagifolia* (AgNPAqF).

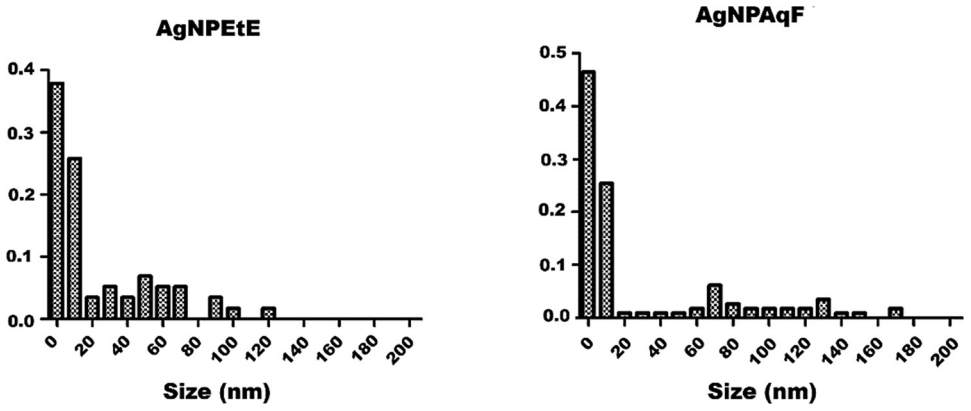

Fig. 9. Histograms of AgNP size (equivalent disc diameter, in nm), from TEM image analysis.

Table 4
Antioxidant activity of AgNPs, Extracts and fractions determined by ABTS, DPPH, FRAP and ORAC assays.

AgNPs/ Extracts	$ABTS^{\cdot+}$ (μgAAE/mL)	DPPH (μgTE/ mL)	FRAP (μgAAE/mL)	ORAC (mmolTE/gExt)
AgNPEtE	72 ± 3	1090 ± 10	759 ± 23	14.6 ± 1.7
AgNPAqF	111 ± 7	210 ± 2	412 ± 79	8 ± 0.8
EtE	61 ± 6	920 ± 10	607 ± 24	6.2 ± 0.03
AqF	83 ± 1	240 ± 2	873 ± 15	9.8 ± 0.9

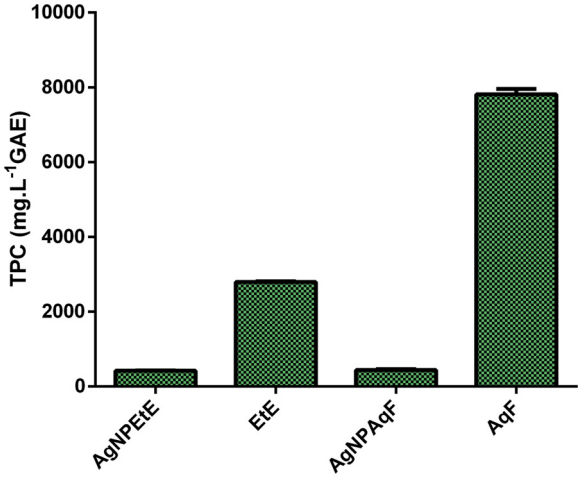

Fig. 10. Total phenolics content-TPC ($mg.L^{-1}$ of acid gallic equivalent) of AgNPs, ethanolic extract (EtE) and aqueous fraction (AqF).

Ag and C atoms is observed with atomic % of 14.5% and 68.9%, respectively. The presence of other elements as well as the intense peak of C can be caused by the existence of organic molecules derived from the extracts and fractions of *T. fagifolia* that are bound to the nanoparticles (Rajesh et al., 2018). The copper in this spectrum likely originates in the TEM grid.

By TEM, the mean size of AgNPEtE was equal to 24.8 ± 29.47 nm and AgNPAqF showed an average size of 30.0 ± 44.60 nm (Fig. 9), following the same tendency of the other techniques (DLS and NTA) in which AgNPAqF presents larger sizes. Beyond the PDI values, the polydispersity of the samples also can be observed in the histograms generated after TEM analysis. Overall, both NTA and DLS indicate considerably higher hydrodynamic diameters than the diameters found in the TEM measurements. This is not surprising, because, as has been discussed elsewhere (Eaton et al., 2017), the two techniques measure very different properties. Indeed, in this work, we expect to have a metal core surrounded by organic material. The methods that measure hydrodynamic diameter (DLS and NTA), would therefore by measuring the whole particle (core and polymeric capping agent), while the TEM would measure only the metallic core. Thus, we can expect, that on average, the metal cores have approximately 20–30 nm in diameter, while on average, an additional 70–80 nm diameter is taken up by the polymeric cores. It is also worth mentioning that light scattering techniques, such as DLS and NTA tend to be more sensitive to larger particles, skewing the data somewhat, and increasing PDI values (Eaton et al., 2017).

3.3. Antioxidant activity

AgNPs are known to have antioxidant properties, and the results obtained for the assessment of the antioxidant activity of synthesized AgNPs are shown in Table 4. In this study, the AgNPAqF demonstrated the highest antioxidant capacity (111 ± 7.3 μg ascorbic acid equivalent/mL) by the ABTS assay. However, this AgNP presented the lowest sequestration of the radical DPPH (210 ± 2 μg Trolox equivalent/mL), similarly to results presented by Abdel-Aziz (2014). The principle of the DPPH-RSA assay is based on the ability of the tested samples to act as donors of hydrogen to the 2,2-diphenyl-1-picrylhydrazyl free radical, this capacity can be attributed to the presence of phenolic compounds and its derivatives, however this assay has some limitations, including greater reactivity in hydrophobic systems: This is unlike the $ABTS^{\cdot+}$ radical, that reacts well in hydrophilic and hydrophobic systems. In addition the $ABTS^{\cdot+}$ may react with more compounds present in the sample than DPPH (Carbonera et al., 2014). Overall, these results demonstrate the importance of using a range of antioxidant activity assays.

Amongst the nanoparticles, AgNPEtE presented the highest FRAP (ferric reduction capacity of plasma) value (759.50 ± 23.38 μg ascorbic acid equivalent/mL) and highest ORAC value (14.6 ± 1.7 mmol Trolox equivalent/g of extract). As expected, the two tests have a good correlation with each other. The ORAC assay has a good correlation with *in vivo* assays and is widely accepted for measuring the total antioxidant capacity of biological samples because it is related to the measurement of a biologically relevant radical (Thaipong et al., 2006). This FRAP value fell by almost half after the synthesis of AgNPAqF (412.40 ± 79.48 μg ascorbic acid equivalent/mL), probably the compounds responsible for the ability to reduce this radical were partially consumed during the synthesis of AgNPs.

The content of total phenolics (TPC), showed in Fig. 10, is related to the antioxidant capacity due to its chemical structure and its reducing properties. The phenolic compounds have an aromatic ring with one or more hydroxyl groups and are present in many plant species. They include several secondary metabolites, such as phenolic acids, flavonoids, coumarins and tannins that, in addition to possessing antioxidant potential, form relatively stable intermediates as a function of the

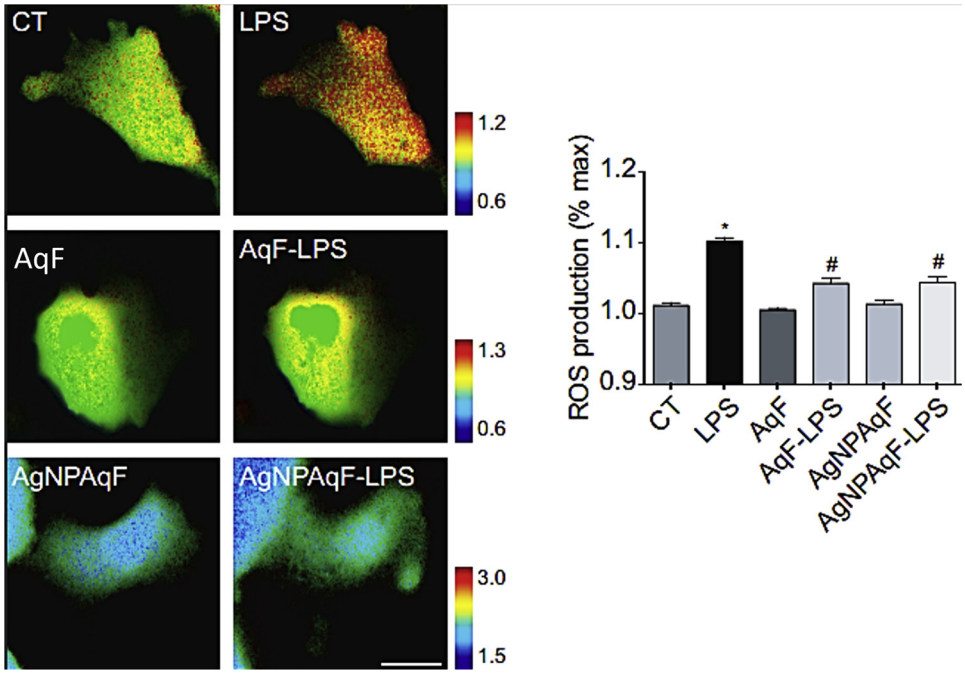

Fig. 11. Silver nanoparticle synthesized with aqueous fraction (AgNPAqF) and aqueous fraction (AqF) prevents ROS generation induced by lipopolysaccharide (LPS) in microglia. CHME3 human microglial cell cultures expressing the ROS biosensor (left) and graph showing the significant increase (*$p < 0.05$) of reactive oxygen species (ROS) in the LPS group *vs*. Control group (CT-saline) and significant decrease ($^{\#}p < 0.05$) of ROS in the groups pretreated with AgNPAqF and AqF *vs* LPS group.

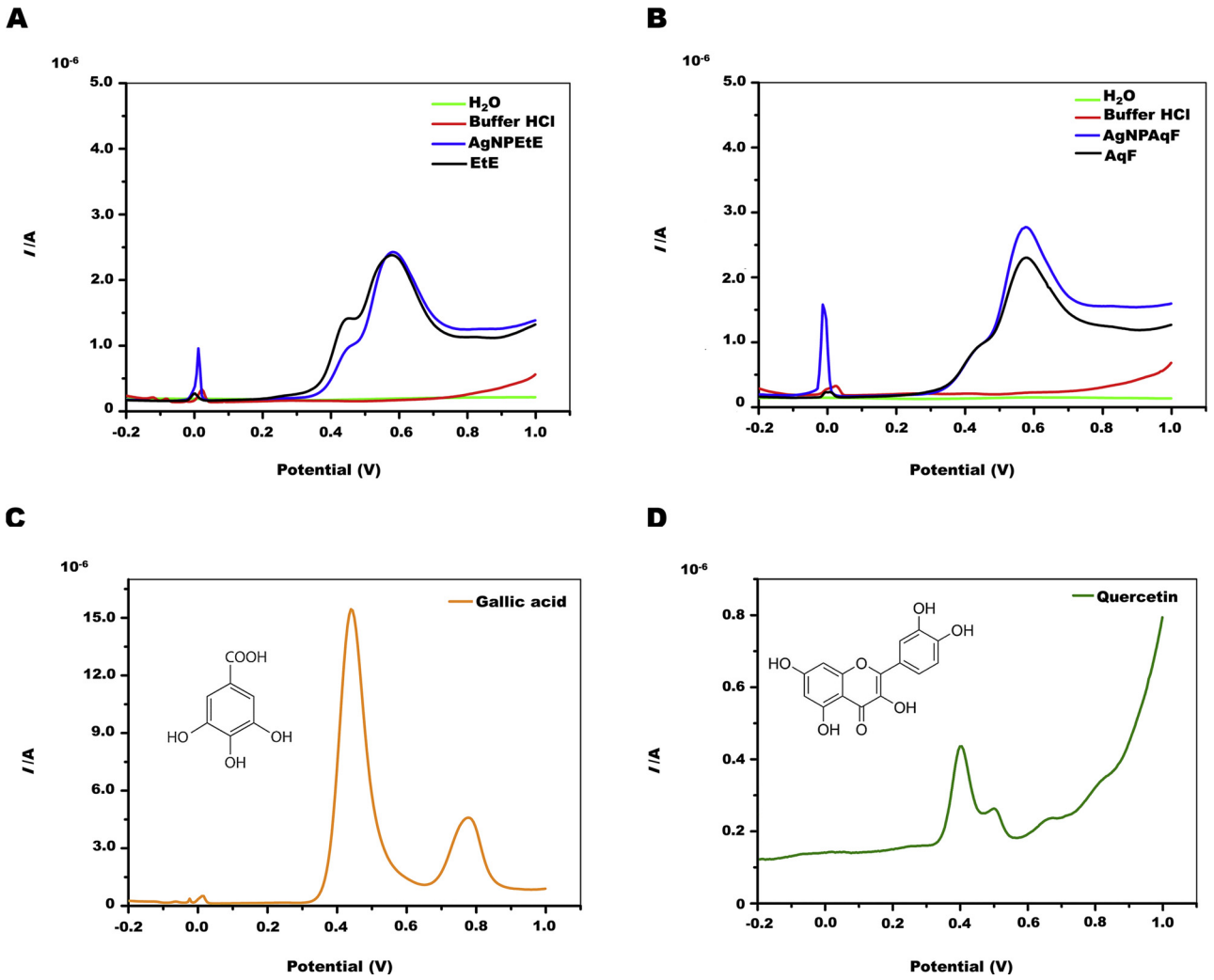

Fig. 12. DPV of AgNPs (**A-D -** blue line), *T. fagifolia* ethanolic extract - EtE or aqueous fraction - AqF (**A-D -** black line), Gallic acid (**E**) and Quercetin (**F**) in 0.1 M HCl (**A-D -** red line) on the electrode.

Table 5
Minimal Inhibitory Concentration (MIC) values of AgNPs, $AgNO_3$ and standard antibacterial (Control) against tested bacteria.

Bacterial strains	AgNPEtE (μgAg/mL)	AgNPAqF (μgAg/mL)	$AgNO_3$ (μg/mL)	Control (μg/mL)
Staphylococcus aureus ATCC 29213	6.75	13.5	13.5	< 0.25[a]
Staphylococcus aureus (MRSA) ATCC 43300	27	27	13.5	< 0.5[b]
Enterococcus faecalis ATCC 29212	6.75	27	6.75	< 4.0[b]
Escherichia coli ATCC 25922	6.75	27	6.75	< 0.5[c]
Pseudomonas aeruginosa ATCC 27853	3.37	27	3.37	< 0.5[c]
Salmonella enterica ATCC 14028	3.37	–	27	< 0.5[c]

Notes: [a] Oxacillin, [b] Vancomycin and [c] Meropenen.

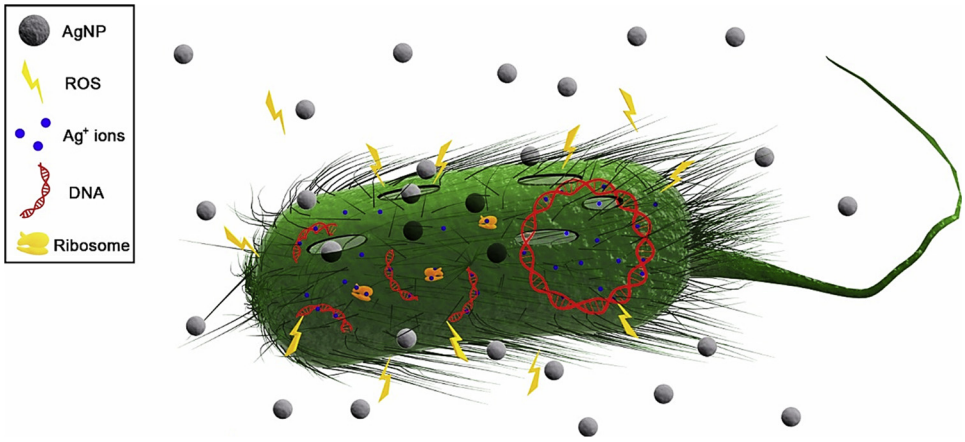

Fig. 13. Proposed mechanisms of the antibacterial activity of *T. fagifolia*-AgNPs. Nanoparticles can cause damage and penetrate the bacterial cell wall and plasma membrane, promote increased generation of reactive oxygen species (ROS), release silver ions (Ag^+) that may also interact with the cell wall and plasma membrane, inhibit replication by binding and fragmentation of bacterial DNA and disrupt protein synthesis (adapted from Durán et al., 2016).

resonance of the aromatic ring present in these substances (Abdel-Aziz et al., 2014; Ignat et al., 2011).

From Fig. 10, it can be seen that the TPC values in plant extract and its aqueous fraction (EtE = 887.40 ± 59.17 and AqF = 826.80 ± 33.07 mg gallic acid equivalent/L) decrease after the synthesis of AgNPs (AgNPEtE = 420.92 ± 9.46 and AgNPAqF = 440.99 ± 21.91 mg gallic acid equivalent/L). This fact may be due to the consumption of these phenolic compounds during the synthesis of AgNPs. The literature reports that the plants of the family Combretaceae, mainly of the genus *Terminalia*, are rich in compounds that induce antioxidant activity (Pfundstein et al., 2010). Therefore, maintenance of amount of these compounds adsorbed to the surface of the nanoparticles can promote antioxidant activity of AgNPs (Patil and Kumbhar, 2017).

Nunes et al. (2014) also measured the TPC of the ethanolic extract (EtE) and aqueous (AqF) fraction of *T. fagifolia* and also found similar values between extract and fraction. The authors also demonstrated the antioxidant capacity of extracts and fractions of *T. fagifolia* by sequestration of DPPH and $ABTS^{\cdot+}$ radicals, corroborating the results found in this study.

The antioxidant capacity of AgNPs synthesized with the aqueous fraction (AgNPAqF) was also evaluated in relation to the generation of lipopolysaccharide (LPS)-induced reactive oxygen species (ROS) in microglial cells, which are implicated in neurodegenerative diseases, such as Parkinson's disease and is a suitable cellular model for this type of study (Barbosa et al., 2018). In Fig. 11 it is possible to observe that LPS (black bar on the graph) promotes a significant increase ($p < 0.05$) in ROS production by microglial cells, when compared to the control group (saline). While the groups pretreated with aqueous fraction (AqF, 125 μg/mL) or AgNPAqF (27 μgAg/mL) showed a significant reduction ($p < 0.05$), when compared to the LPS group. Gonzalez-Carter et al. (2017) also demonstrated reduction of LPS-induced ROS by silver nanoparticles in the microglial cell model, as well as the absence of AgNP toxicity on these cells.

3.4. Electrochemical profile analysis

Differential pulse voltammetry (DPV) was used to observe the electrochemical behaviour of the AgNPs. Using screen printed carbon electrodes (SCPEs) as the electrochemical platform, the electrical measurements were performed over the potential range of -0.20 to + 1.0 V. Typical anodic potential peaks at around + 00,114 V and + 00,137 V were observed for the AgNPEtE (Fig. 12A) and AgNPAqF (Fig. 12B), respectively. It was reported these electrochemical oxidation peaks correspond to the electrochemical oxidation of the Ag^0, present in the AgNPs, to Ag^+ (Ivanova and Zamborini, 2010). Moreover, other two oxidation electrochemical peaks at potential of + 0.43 V and + 0.58 V were also observed, these peaks can be attributed to the oxidation of different polyphenolic and flavonoids compounds which are present in the plant derivatives, similar to gallic acid and quercetin (Fig. 12C and D). The presented electrochemical profiles presuppose the antioxidant potential presented previously.

3.5. Antibacterial activity

The synthetized AgNPs were tested against six bacterial strain, three Gram-positive (*Staphylococcus aureus, Staphylococcus aureus* MRSA and *Enterococcus faecalis*) and three Gram-negative (*Escherichia coli, Pseudomonas aeruginosa* and *Salmonella enterica* serovar Typhimurium) with clinical relevance due to high prevalence in human infections (WHO, 2018). All AgNPs showed activity against sensitive and resistant Gram-positive bacteria (MICs ranging from 6.75 to 27 μgAg/mL) as well as ethanolic extract and aqueous fraction. For Gram-negative bacteria the MICs ranged from 3.37 to 27 μgAg/mL, AgNPAqF did not inhibit the growth of *S. enterica* (Table 5). It is important to clarify that nanoparticles precursors (extract and fraction) are not active against Gram-negative bacteria (Araújo et al., 2015)

In general, AgNPEtE presented the best antibacterial result with *P. aeruginosa* and *S. enterica* being the most sensitives strains with MIC values of 3.37 μgAg/mL. Possibly, the AgNPs interact more strongly with the lipopolysaccharides of Gram-negative bacteria (Shrivastava

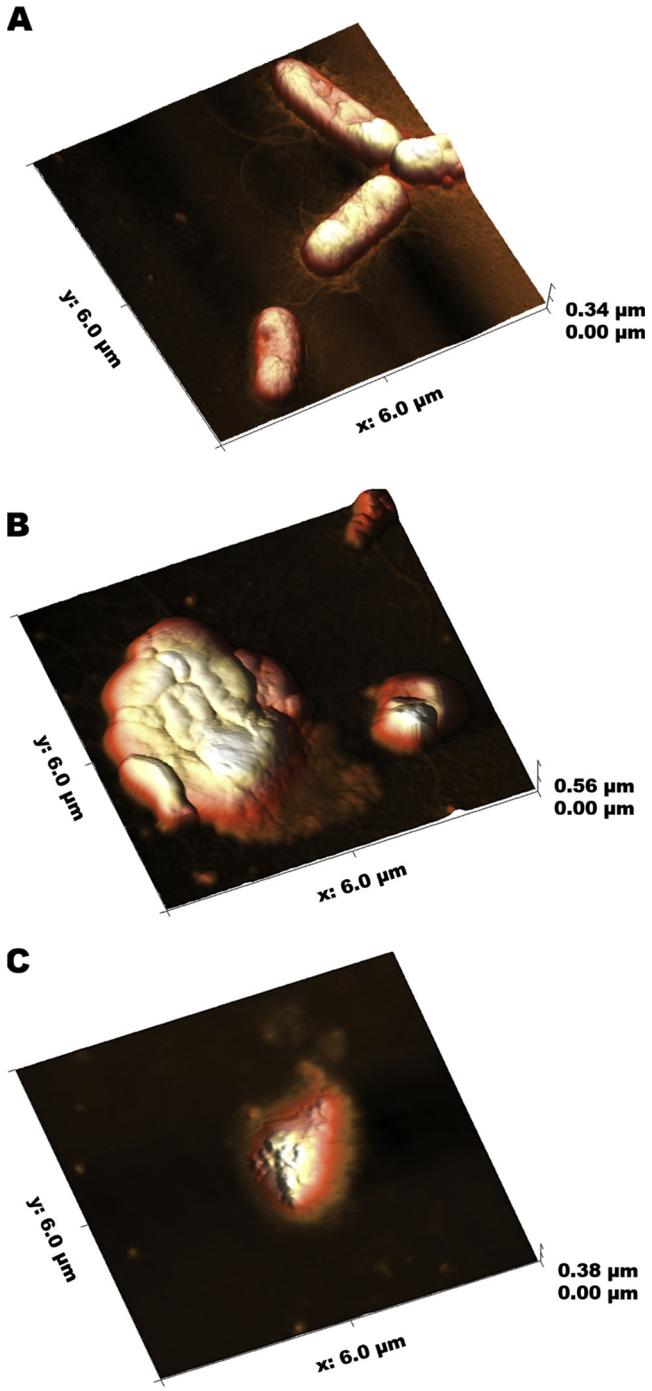

Fig. 14. AFM height images of *Escherichia coli* ATCC 25922. **A**) *E. coli* untreated (control); **B**) *E. coli* treated at sub-MIC concentration of AgNPEtE and **C**) *E. coli* treated at MIC concentration of AgNPEtE.

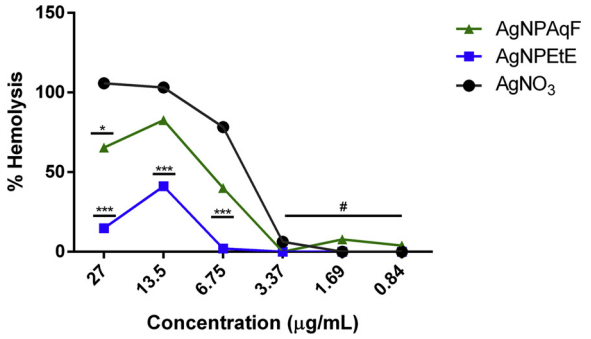

Fig. 15. Percentage of haemolysis induced by AgNPs and $AgNO_3$ at different concentrations.*** for $p < 0.001$/* for $p < 0.05$ and # for no significance.

et al., 2007). It is also notable that, with exception of *S. aureus* MRSA (resistant bacteria), AgNPEtE was able to inhibit all strains at concentrations below 10 µgAg/mL. AgNPEtE showed one of the smallest average size of the particles (Table 3) and spherical shape (Fig. 7A/B) which may have contributed to the best antibacterial effect, because increases surface area and, consequently, the contact with microorganisms. In spite of showing good sensitivity to AgNPEtE, the Gram-negative strain *S. enterica* was the only strain that did not show sensitivity to all AgNPs (AgNPAqF). The literature shows some cases of silver-resistant bacteria, generally, this type of resistance is associated with the bacterial habitat and with aggregation of nanoparticles (Durán et al., 2016; Panáček et al., 2018).

Bacteria of the genus *Staphylococcus* sp. were susceptible to the AgNPs tested; however, methicillin-resistant *S. aureus* (MRSA) was less sensitive. Besides being an important virulence factor in the establishment and development of infections caused by *S. aureus*, Methicillin resistance is becoming increasingly prevalent (Garza-González and Dowzicky, 2013). $AgNO_3$ also showed antibacterial activity against tested strains, in some cases the activity was better than AgNPs, as results also found by Li et al. (2017). On the other hand Panáček et al. (2018) report that nanoparticles synthesized with pomegranate rind extract (which has composition similar to EtE and AqF) may suppress the development of bacterial resistance as well as stabilize and prevent the aggregation of nanoparticles.

Upon contact with bacteria, AgNPs can act by several killing mechanisms, to cause rupture of the cell wall, to increase the permeability of the membrane, interfering in protein synthesis, or prolonging the lag phase. The release of Ag^+ ions promotes the interaction of these ions with the bacterial DNA, causing DNA fragmentation by intercalation between the bases and breaking of the hydrogen bonds, that maintains the double strand of DNA intact (Li et al., 2017; Sondi and Salopek-Sondi, 2004).

Treatment with AgNPs may lead to pore formation in the bacterial membrane, increasing the permeability to Ag cations; however, the intrinsic antibacterial activity does not only depend on it. AgNPs are assumed to increase the amount of reactive oxygen species (ROS) in the bacterial cell environment. Nanoparticles have a great reactivity in addition to lower tendency to induce microbial resistance (Hwang et al., 2008; Park et al., 2009). The cited mechanisms are illustrated in Fig. 13.

For confirmation of the morphological changes details that AgNPEtE promotes on *E. coli* ATCC 25922, atomic force microscopy was performed and the images are showed in Fig. 14. The control cells showed characteristics of rod-shaped bacteria (Fig. 14A), in contrast, after exposure to sub-MIC concentration of AgNPEtE (3.37 µg/mL) for 24 h, the

Table 6
Minimal Inhibitory Concentrations (MICs) values of AgNPs, $AgNO_3$ and itraconazole against tested fungi.

Fungal strains	AgNPEtE (µgAg/mL)	AgNPAqF (µgAg/mL)	$AgNO_3$ (µg/mL)	Itraconazole (µg/mL)
Candida krusei ATCC 6258	0.10	0.21	0.10	0.12
Tricophyton interdigitale ATCC 75826	1.69	1.69	0.84	0.12
Fonsecaea pedrosoi ATCC 46428	6.75	6.75	27	0.25

image reveals increase in cell surface roughness and decrease in cell height and indentations. Very few distinct bacilli were seen. Probably cell wall and membrane damage occurred and the cells were then deformed with apparent collapse of bacterial cells (Fig. 14B).

After exposure to 6.75 μg/mL of AgNPEtE (MIC concentration) for 24 h the cell morphology changed irreversibly with total loss of rod shape. In summary, the *E. coli* appeared to be destroyed completely (Fig. 14C). AgNPs might destabilize the outer membrane, collapse the plasma membrane potential, deplete the levels of intracellular ATP and lead to pore formation, culminating in cell lysis (Składanowski et al., 2017).

3.6. Antifungal activity

Increased survival of immunocompromised patients has led to an increase in the incidence of fungal infections; therefore it is necessary to develop new therapeutic alternatives. The AgNPs were also tested for their ability to inhibit fungal growth against a yeast, *Candida krusei* and two filamentous fungi, *Tricophyton interdigitale* e *Fonsecaea pedrosoi*. The nanoparticles exhibited strong antifungal activity with MICs ranging from 0.10 to 6.75 μgAg/mL (Table 6). *C. krusei* yeast, recognized for intrinsic resistance, was the most sensitive strain to the action of AgNPs, however it is important to emphasize that the filamentous fungi used in this study are difficult to treat and have become resistant to antifungal agents used in clinical practice (Tamura et al., 2014; Vandeputte et al., 2012).

It is reported in the literature that AgNPs have inhibitory activity on yeasts of the genus *Candida* sp. by altering the membrane potential, forming pores, and releasing the cytoplasmic content, similar to the mechanism of action for bacteria (Kim et al., 2009). Another important mechanism of action is the increased reactive oxygen species which are converted inside the fungal cell into the strong oxidant $^{\cdot}OH$ (hydroxyl radicals) leading to a reduction in the mitochondrial membrane potential and the release of cytochrome c from mitochondria resulting in apoptosis (Hwang et al., 2012).

This is the first time that silver nanoparticles have been tested against *F. pedrosoi*, the etiologic agent of chromoblastomycosis (Queiroz-Telles et al., 2017), however studies against another filamentous fungus reveals that AgNPs may interfere in the fungal reproduction process and cause structural changes in hyphae (Lamsal et al., 2011). Rónavári et al. (2018) showed in their study that silver nanoparticles were able to reduce the diameter of the colony of *Tricophyton* sp. with 30 μg/mL, but did not show the same effect with 10 μg/mL, whereas in our study the MIC of the AgNPs for *T. interdigitale* was much lower, ranging from 0.21 to 1.69 μg/mL.

Chromoblastomycosis is a polymorphic fungal disease defined by the implantation of the fungus that leads to a hyperproliferation of host tissue, combined with the presence of a pathogenic fungal phase in the form of muriform cells. This infection presents as a chronic, granulomatous infection of the skin and subcutaneous tissue and may present secondary infection, which is responsible for the morbidity of this disease, together with the inability of the affected part of the body or the transformation of the squamous cells into carcinoma (Daboit et al., 2014; Queiroz-Telles et al., 2017).

We obtained a MIC value of 6.75 μg/mL for *Fonsecaea pedrosoi*, a fungal genus that is considered as the most common in Brazil. Infections (chromoblastomycosis) caused by *F. pedrosoi* can be more difficult to treat than from others species. In regards to the chromoblastomycosis, which is one of the fungal implantations more prevalent, its melanin confers to them a virulence factor what make them more resistant than others fungi. The therapy is long and is related to a low cure ratio (Bonifaz et al., 2004; Daboit et al., 2014; Queiroz-Telles et al., 2017).

3.7. Biocompatibility test

After demonstrating the antimicrobial and antioxidant potential of AgNPs, testing for lysis of red blood cells following exposure to silver nanoparticles is relevant because AgNPs may translocate into the circulatory system by several routes (Huang et al., 2016). In our biocompatibility study, red blood cells (RBCs) were exposed to AgNPs (0.84–27 μg/mL) and the result is shown in Fig. 15.

AgNPEtE was the most biocompatible nanoparticle among the AgNPs tested as it presented lower than 15% of haemolysis at the highest concentration tested, followed by AgNPAqF that presented around 65% of haemolysis at the concentration of 27 μg/mL, while $AgNO_3$ promoted 100% haemolysis at this same concentration. At the concentration of 6.75 μg/mL $AgNO_3$ promoted about 80% haemolysis, compared to AgNPEtE that presented < 5% haemolysis. Ruden et al. (2009) obtained a similar result when comparing the haemolytic activity of silver nanoparticles to that of $AgNO_3$. The substances tested were not able to promote haemolysis at concentrations ≤ 3.37 μg/mL. It is important to emphasize that AgNPEtE was active against all strains of microorganisms used in concentrations below 13.5 μg/mL, and therefore was biocompatible at the effective concentrations. The AgNPAqF also showed antibacterial and antifungal activity at non-toxic concentrations.

The haemolytic effect promotes the rupture of erythrocytes (RBCs) and the release of their contents of haemoglobin by compromising membrane integrity and surface characteristics. Such changes can be induced by the release of oxidative stress products following exposure to AgNPs, but the exact mechanism for RBC membrane damage is not yet clear. Probably the antioxidant capacity (see Table 3) of the AgNPs influenced the biocompatibility of the nanoparticles (Huang et al., 2016).

4. Conclusion

Eschweilenol C was identified for the first time in an extract of the species *T. fagifolia* Mart.. The ethanolic extract and its aqueous fraction were effective in the environmentally benign synthesis of silver nanoparticles with significant antioxidant, antibacterial and antifungal activity. For the first time, the inhibitory action of silver nanoparticles against the pathogenic fungus *Fonsecaea pedrosoi* was shown. He synthesised AgNPs also showed good biocompatibility, especially in relation to $AgNO_3$, and may be promising alternatives in the medical field with various industrial applications, with low environmental impact.

Conflict of interest

There are no conflicts to declare.

Acknowledgments

We thank Herbert Kogler and Reinhard Wimmer for the identification of Eschweilenol C. The NMR laboratory at Aalborg University is supported by the Obel Family, SparNord and Carlsberg foundations. The authors are grateful to Carla Eiras (LIMAV/CT/UFPI) and to FCT and EU for financial support through project UID/QUI/50006/2013–POCI-01-0145-FEDER-007265 from COMPETE and project NORTE-01-0145-FEDER-000011 from COMPETE. Thanks to Andreia Pinto for help with the TEM measurements at Instituto de Medicina Molecular (IMM). This work was supported by the Histology and Comparative Pathology Laboratory of the IMM.

References

Abdel-Aziz, M.S., Shaheen, M.S., El-Nekeety, A.A., Abdel-Wahhab, M.A., 2014. Antioxidant and antibacterial activity of silver nanoparticles biosynthesized using Chenopodium murale leaf extract. J. Saudi Chem. Soc. 18, 356–363. https://doi.org/10.1016/j.jscs.2013.09.011.

Araújo, A.R., Quelemes, P.V., Perfeito, M.L.G., Lima, L.I., Sá, M.C., Nunes, P.H.M., Joanitti, G.A., Eaton, P., Soares, M.J.S., Leite, J.R.S.A., 2015. Antibacterial, antibiofilm and cytotoxic activities of Terminalia fagifolia Mart. extract and fractions.

Ann. Clin. Microbiol. Antimicrob. 14, 25–35. https://doi.org/10.1186/s12941-015-0084-2.
Asami, Y., Ogura, T., Otake, N., Nishimura, T., Xinsheng, Y., Sakurai, T., Nagasawa, H., Sakuda, S., Tatsuta, K., 2003. Isolation and synthesis of a new bioactive ellagic acid derivative from Combretum yunnanensis. J. Nat. Prod. 66, 729–731. https://doi.org/10.1021/np030041j.
Barbosa, E.A., Oliveira, A., Plácido, A., Socodato, R., Portugal, C.C., Mafud, A.C., Ombredane, A.S., Moreira, D.C., Vale, N., Bessa, L.J., Joanitti, G.A., Alves, C., Gomes, P., Delerue-Matos, C., Mascarenhas, Y.P., Marani, M.M., Relvas, J.B., Pintado, M., Leite, J.R.S.A., 2018. Structure and function of a novel antioxidant peptide from the skin of tropical frogs. Free Radic. Biol. Med. 115, 68–79. https://doi.org/10.1016/j.freeradbiomed.2017.11.001.
Barroso, M.F., Ramalhosa, M.J., Alves, R.C., Dias, A., Soares, C.M.D., Oliva-Teles, M.T., Delerue-Matos, C., 2016. Total antioxidant capacity of plant infusions: assessment using electrochemical dna-based biosensor and spectrophotometric methods. Food Control 68, 153–161. https://doi.org/10.1016/j.foodcont.2016.03.029.
Bonifaz, A., Paredes-Solis, V., Saul, A., 2004. Treating chromoblastomycosis with systemic antifungals. Expert Opin. Pharmacol. 5, 247–254. https://doi.org/10.1517/14656566.5.2.247.
Carbonera, F., Montanher, P.F., Palombini, S.V., Maruyama, S.A., Claus, T., Santos, H.M.C., Sargi, S.C., Matsushitaa, M., Visentainer, J.V., 2014. Antioxidant capacity in tilapia fillets enriched with extract of acerola fruit residue. J. Braz. Chem. Soc. 25, 1237–1245. https://doi.org/10.5935/0103-5053.20140101. 2014.
CLSI - Clinical Laboratory Standards Institute, 2008a. Approved Standard M38–A2. Wayne, Pa.
CLSI - Clinical Laboratory Standards Institute, 2008b. Approved Standard M27–A3. Wayne, Pa.
CLSI - Clinical Laboratory Standards Institute, 2012. Approved Standard M07–A9. Wayne, Pa.
Cock, I.E., 2015. The medicinal properties and phytochemistry of plants of the genus *Terminalia* (Combretaceae). Inflammopharmacology 23, 203–229. https://doi.org/10.1007/s10787-015-0246-z.
Daboit, T.C., Magagnin, C.M., Heidrich, D., Antochevis, L.C., Vigolo, S., Meirelles, L.C., Alves, K., Scroferneker, M.L., 2014. In vitro susceptibility of chromoblastomycosis agents to five antifungal drugs and to the combination of terbinafine and amphotericin B. Mycoses 57, 116–120. https://doi.org/10.1111/myc.12111.
Durán, N., Durán, M., Jesus, M.B., Seabra, A.B., Fávaro, W.J., Nakazato, G., 2016. Silver nanoparticles: a new view on mechanistic aspects on antimicrobial activity. Nanomedicine 12, 789–799. https://doi.org/10.1016/j.nano.2015.11.016.
Eaton, P., Quaresma, P., Soares, C., Neves, C.S., de Almeida, M.P., Pereira, E., West, P., 2017. A direct comparison of experimental methods to measure dimensions of synthetic nanoparticles. Ultramicroscopy 182, 179–190. https://doi.org/10.1016/j.ultramic.2017.07.001.
Edison, T.N.J.I., Lee, Y.R., Sethuraman, M.G., 2016. Green synthesis of silver nanoparticles using *Terminalia cuneata* and its catalytic action in reduction of direct yellow-12 dye. Spectrochim. Acta A 161, 122–129. https://doi.org/10.1016/j.saa.2016.02.044.
Garza-González, E., Dowzicky, M.J., 2013. Changes in *Staphylococcus aureus* susceptibility across Latin America between 2004 and 2010. Braz. J. Infect. Dis. 17, 13–19. https://doi.org/10.1016/j.bjid.2012.08.017.
Gião, M.S., Gonzalez-Sanjose, M.L., Rivero-Perez, M.D., Pereira, C.I., Pintado, M.E., Malcata, F.X., 2007. Infusions of Portuguese medicinal plants: dependence of final antioxidant capacity and phenol content on extraction features. J. Sci. Food Agric. 87, 2638–2647. https://doi.org/10.1002/jsfa.3023.
Gonzalez-Carter, D.A., Leo, B.F., Ruenraroengsak, P., Chen, S., Goode, A.E., Theodorou, I.G., Chung, K.F., Carzaniga, R., Shaffer, M.S.P., Dexter, D.T., Ryan, M.P., Porter, A.E., 2017. Silver nanoparticles reduce brain inflammation and related neurotoxicity through induction of H2S-synthesizing enzymes. Sci Rep. 7, 42871–42884. https://doi.org/10.1038/srep42871.
Huang, D., Ou, B., Hampsch-Woodill, M., Flanagan, J., Prior, J.-R., 2002. High-throughput assay of oxygen radical absorbance capacity (ORAC) using a multichannel liquid handling system coupled with a microplate fluorescence reader in 96-well format. J. Agric. Food Chem. 50, 4437–4444. https://doi.org/10.1021/jf0201529.
Huang, H., Lai, W., Cui, M., Liang, L., Lin, Y., Fang, Q., Liu, Y., Xie, L., 2016. An evaluation of blood compatibility of silver nanoparticles. Sci. Rep. 6, 1–15. https://doi.org/10.1038/srep25518.
Hwang, E.T., Lee, J.H., Chae, Y.J., Kim, Y.S., Kim, B.C., Sang, B.-I., Gu, M.B., 2008. Analysis of the toxic mode of action of silver nanoparticles using stress-specific bioluminescent bacteria. Small 4, 746–750. https://doi.org/10.1002/smll.200700954.
Hwang, I.-S., Lee, J., Hwang, J.-H., Kim, K.-J., Lee, D.G., 2012. Silver nanoparticles induce apoptotic cell death in Candida albicans through the increase of hydroxyl radicals. FEBS J. 279, 1327–1338. https://doi.org/10.1111/j.1742-4658.2012.08527.x.
Ignat, I., Volf, I., Popa, V.I., 2011. A critical review of methods for characterization of polyphenolic compounds in fruits and vegetables. Food Chem. 126 (1821-), 1835. https://doi.org/10.1016/j.foodchem.2010.12.026.
Ivanova, O.S., Zamborini, F.P., 2010. Size-dependent electrochemical oxidation of silver nanoparticles. J. Am. Chem. Soc. 132, 70–72. https://doi.org/10.1021/ja908780g.
Kalishwaralal, K., Deepak, V., Pandian, R.K., Barathmani, S.M.K., Kartikeyan, K.S., Gurunathan, B.S., 2010. Biosynthesis of silver and gold nanoparticles using Brevibacterium casei. Colloids Surf. B: Biointerfaces 77, 257–262. https://doi.org/10.1016/j.colsurfb.2010.02.007.
Kim, K.-J., Sung, W.S., Suh, B.K., Moon, S.-K., Choi, J.-S., Kim, J.G., Lee, D.G., 2009. Antifungal activity and mode of action of silver nanoparticles on Candida albicans. Biometals 22, 235–242. https://doi.org/10.1007/s10534-008-9159-2.
Kuppusamy, P., Yusoff, M.M., Maniam, G.P., Govindan, N., 2016. Biosynthesis of metallic nanoparticles using plant derivatives and their new avenues in pharmacological applications—an updated report. Saudi Pharm. J. 24, 473–484. https://doi.org/10.1016/j.jsps.2014.11.013.
Lamsal, K., Kim, S.W., Jung, J.H., Kim, Y.S., Kim, Y.S., Lee, Y.S., 2011. Application of silver nanoparticles for the control of colletotrichum species in vitro and pepper anthracnose disease in field. Mycobiology 39, 194–199. https://doi.org/10.5941/MYCO.2011.39.3.194.
Li, X.-C., Elsohly, H.N., Hufford, C.D., Clark, A.M., 1999. NMR assignments of ellagic acid derivatives. Magn Reson Chem. 37, 856–859. https://doi.org/10.1002/(SICI)1097-458X(199911)37:11<856::AID-MRC529>3.0.CO;2-X.
Li, W.R., Sun, T.-L., Zhou, S.-L., Ma, Y.-K., Shi, Q.-S., Xie, X.-B., Huang, X.-M., 2017. A comparative analysis of antibacterial activity, dynamics, and effects of silver ions and silver nanoparticles against four bacterial strains. Int. Biodeterior. Biodegr. 123, 304–310. https://doi.org/10.1016/j.ibiod.2017.07.015.
Lin, J., Nishino, K., Roberts, M.C., Tolmasky, M., Aminov, R.I., Zhang, L., 2015. Mechanisms of antibiotic resistance. Front. Microbiol. 6, 1–3. https://doi.org/10.3389/fmicb.2015.00034.
MacCuspie, R.I., Rogers, K., Patra, M., Suo, Z., Allen, A.J., Martin, M.N., Hackley, V.A., 2011. Challenges for physical characterization of silver nanoparticles under pristine and environmentally relevant conditions. J. Environ. Monit. 13, 1212–1226. https://doi.org/10.1039/c1em10024f.
Marani, M.M., Perez, L.O., Araujo, A.R., Plácido, A., Sousa, A.C., Quelemes, P.V., Oliveira, M., Gomes-Alves, A., Pueta, M., Gameiro, P., Tomás, A.M., Delerue-Matos, C., Eaton, P., Camperi, S.A., Basso, N.G., Leite, J.R.S.A., 2016. Thaulin-1: the first antimicrobial peptide isolated from the skin of a Patagonian frog pleurodema thaul (Anura: leptodactylidae: leiuperinae) with activity against Escherichia coli. Gene 20, 70–80. https://doi.org/10.1016/j.gene.2016.12.020.
Mulvaney, P., 1996. Surface plasmon spectroscopy of nanosized metal particles. Langmuir 12, 788–800. https://doi.org/10.1021/la9502711.
Nunes, P.H.M., Martins, M.C.C., Oliveira, R.C.M., Chaves, M.H., Sousa, E.A., Leite, J.R.S.A., Véras, L.M., Almeida, F.R.C., 2014. Gastric antiulcerogenic and hypokinetic activities of Terminalia fagifolia Mart. & Zucc. (Combretaceae). Biomed. Res. Int. 1–15. https://doi.org/10.1155/2014/261745.
Paczkowska, M., Lewandowska, K., Bednarski, W., Mizera, M., Podborska, A., Krause, A., Cielecka-Piontek, J., 2015. Application of spectroscopic methods for identification (FT-IR, Raman spectroscopy) and determination (UV, EPR) of quercetin-3-Orutinoside. Experimental and DFT based approach. Spectrochim. Acta A Mol. Biomol. Spectrosc. 140, 132–139. https://doi.org/10.1016/j.saa.2014.12.050.
Panáček, A., Kvítek, L., Smékalová, M., Večeřová, R., Kolář, M., Röderová, M., Dyčka, F., Šebela, M., Prucek, R., Tomanec, O., Zbořil, R., 2018. Bacterial resistance to silver nanoparticles and how to overcome it. Nat. Nanotechnol. 13, 65–71. https://doi.org/10.1038/s41565-017-0013-y.
Park, H.J., Kim, J.Y., Kim, J., Lee, J.-H., Hahn, J.-S., Gu, M.B., Yoon, J., 2009. Silver-ion-mediated reactive oxygen species generation affecting bactericidal activity. Water Res. 43, 1027–1032. https://doi.org/10.1016/j.watres.2008.12.002.
Patil, S.P., Kumbhar, S.T., 2017. Antioxidant, antibacterial and cytotoxic potential of silver nanoparticles synthesized using terpenes rich extract of Lantana camara L. leaves. Biochem. Biophys. Rep. 10, 76–81. https://doi.org/10.1016/j.bbrep.2017.03.002.
Pfundstein, B., El Desouky, S.K., Hull, W.E., Haubner, R., Erben, G., Owen, R.W., 2010. Polyphenolic compounds in the fruits of Egyptian medicinal plants (Terminalia bellerica, Terminalia chebula and Terminalia horrida): characterization, quantitation and determination of antioxidant capacities. Phytochemistry 71, 1132–1148. https://doi.org/10.1016/j.phytochem.2010.03.018.
Queiroz-Telles, F., Hoog, S., Santos, D.W.C., Salgado, C.G., Vicente, V.A., Bonifaz, A., Roilides, E., Xi, L., Azevedo, C.M., Silva, M.B., Pana, Z.D., Colombo, A.L., Walsh, T.J., 2017. Chromoblastomycosis. Clin. Microbiol. Ver. 30, 233–276.
Quelemes, P.V., Araruna, F.B., Faria, B.E.F., Kuckelhaus, S.A.S., Silva, D.A., Mendonça, R.Z., Eiras, C., Soares, M.J.S., Leite, J.R.S.A., 2013. Development and antibacterial activity of cashew gum-based silver nanoparticles. Int. J. Mol. Sci. 14, 4969–4981.
Rajesh, K.M., Ajitha, B., Reddy, Y.A.K., Suneetha, Y., Reddy, P.S., 2018. Assisted green synthesis of copper nanoparticles using Syzygium aromaticum bud extract: physical, optical and antimicrobial properties. Optik 154, 593–600.
Rajeshkumar, S., Malarkodi, C., Gnanajobitha, G., Paulkumar, K., Vanaja, M., Kannan, C., Annadurai, G., 2013. Seaweed-mediated synthesis of gold nanoparticles using Turbinaria conoides and its characterization. J. Nanostruct. Chem. 44, 1–7.
Rasheed, W., Shah, M.R., Perveen, S., Ahmed, S., Uzzaman, S., 2018. Revelation of susceptibility differences due to Hg(II) accumulation in Streptococcus pyogenes against CX-AgNPs and Cefixime by atomic force microscopy. Ecotoxicol. Environ. Saf. 147, 9–16. https://doi.org/10.1016/j.ecoenv.2017.08.030.
Rónavári, A., Igaz, N., Gopisetty, M.K., Szerencsés, B., Kovács, D., Papp, C., Vágvölgyi, C., Boros, I.M., Kónya, Z., Kiricsi, M., Pfeiffer, I., 2018. Biosynthesized silver and gold nanoparticles are potent antimycotics against opportunistic pathogenic yeasts and dermatophytes. Int. J. Nanomed. 13, 695–703.
Ruden, S., Hilpert, K., Berditsch, M., Wadhwani, P., Ulrich, A.S., 2009. Synergistic interaction between silver nanoparticles and membrane-permeabilizing antimicrobial peptides. Antimicrob. Agents Chemother. 53, 3538–3540.
Salem, J.K., El-Nahhal, I.M., Najri, B.A., Hammad, T.M., 2016. Utilization of surface Plasmon resonance band of silver nanoparticles for determination of critical micelle concentration of cationic surfactants. Chem. Phys. Lett. 664, 154–158.
Salopek, B., Krasi, D., Filipovi, S., 1992. Measurement and application of zeta-potential. Rudarsko-geolosko-naftni zbornik 4, 147–151.
Shrivastava, S., Bera, T., Roy, A., Singh, G., Ramachandrarao, P., Dash, D., 2007. Characterization of enhanced antibacterial effects of novel silver nanoparticles.

Nanotechnology 18, 1–9. https://doi.org/10.1088/0957-4484/18/22/225103.
Składanowski, M., Wypij, M., Laskowski, D., Golińska, P., Dahm, H., Rai, M., 2017. Silver and gold nanoparticles synthesized from Streptomyces sp. isolated from acid forest soil with special reference to its antibacterial activity against pathogens. J. Clust. Sci. 28, 59–79. https://doi.org/10.1007/s10876-016-1043-6.
Sondi, I., Salopek-Sondi, B., 2004. Silver nanoparticles as antimicrobial agent: a case study on E. coli as a model for Gram-negative bacteria. J. Colloid Interface Sci. 275, 177. https://doi.org/10.1016/j.jcis.2004.02.012.
Stavis, S.M., Fagan, J., Stopa, M., Liddle, J.A., 2018. Nanoparticle manufacturing – heterogeneity through processes to products. ACS Appl. Nano Mater. 1, 4358–4385. https://doi.org/10.1021/acsanm.8b01239.
Suman, T.Y., Elumalai, D., Kaleena, P.K., Rajasreea, S.R.R., 2013. GC–MS analysis of bioactive components and synthesis of silver nanoparticle using Ammannia baccifera aerial extract and its larvicidal activity against malaria and filariasis vectors. Ind. Crop. Prod. 47, 239–245. https://doi.org/10.1016/j.indcrop.2013.03.010.
Sun, Q., Cai, X., Li, J., Zheng, M., Chenb, Z., Yu, C.P., 2014. Green synthesis of silver nanoparticles using tealeaf extract and evaluation of their stability and antibacterial activity. Colloid Surf. A: Physicochem Eng. Aspects 444, 226–231. https://doi.org/10.1016/j.colsurfa.2013.12.065.
Tamura, T., Asahara, M., Yamamoto, M., Yamaura, M., Matsumura, M., Goto, K., Rezaei-Matehkolaei, A., Mirhendi, H., Makimura, M., Makimura, K., 2014. In vitro susceptibility of dermatomycoses agents to six antifungal drugs and evaluation by fractional inhibitory concentration index of combined effects of amorolfine and itraconazole in dermatophytes. Microbiol. Immunol. 58, 1–8. https://doi.org/10.1111/1348-0421.12109.
Thaipong, K., Boonprakob, U., Crosby, K., Cisneros-Zevallosc, L., Byrne, D.H., 2006. Comparison of ABTS, DPPH, FRAP, and ORAC assays for estimating antioxidant activity from guava fruit extracts. J. Food Compos. Anal. 19, 669–675. https://doi.org/10.1016/j.jfca.2006.01.003.
Tolaymat, T.M., El Badawy, A.M., Genaidy, A., Scheckel, K.G., Luxton, T.P., Suidan, M., 2010. An evidence-based environmental perspective of manufactured silver nanoparticle in syntheses and applications: a systematic review and critical appraisal of peer-reviewed scientific papers. Sci. Total Environ. 5, 999–1006. https://doi.org/10.1016/j.scitotenv.2009.11.003.
Vandeputte, P., Ferrari, S., Coste, A.T., 2012. Antifungal resistance and new strategies to control fungal infections. Int. J. Microbiol. 2012, 1–26. https://doi.org/10.1155/2012/713687.
WHO – World Health Oganization, 2018. Antimicrobial resisTance. (Accessed 29 July 2018). http://www.who.int/mediacentre/factsheets/fs194/en/.
Yang, S.-W., Zhou, B.-N., Wisse, J.H., Evans, R., van der Werff, H., Miller, J.S., Kingston, D.G.I., 1998. Three new ellagic acid derivatives from the bark of Eschweilera coriacea from the Suriname Rainforest. J. Nat. Prod. 61, 901–906. https://doi.org/10.1021/np980046u.